



## Modeling radiative heating of liquids in microchip reaction chambers

Christopher R. Phaneuf\*, Nikita Pak, Craig R. Forest

Georgia Institute of Technology, Department of Mechanical Engineering, Atlanta, GA 30332, USA

### ARTICLE INFO

#### Article history:

Received 3 March 2010

Received in revised form 25 January 2011

Accepted 2 February 2011

Available online 26 February 2011

#### Keywords:

Microfluidics

Heat transfer

Temperature control

Radiative heating

Finite element

### ABSTRACT

Deterministic design of a microfluidic system that utilizes radiative heating requires accurate thermal modeling. Current modeling methods are limited to describing a subset of the spatial and spectral parameter space and thus cannot be extended to the full range of microchip platforms. This paper presents a broadly applicable approach to modeling the thermal response of liquid undergoing radiative heating in microchip reaction chambers by using optical and material properties for analytical and finite element methods. The fidelity of the model is demonstrated with experimental validation for two types of microchips, glass and plastic, and two types of radiative sources, blackbody and monochromatic, revealing root mean square deviations between 1.37 °C and 3.14 °C. By providing an understanding of how a radiative source interacts with a particular device and the resulting transient and steady state behavior, this modeling process can enable designs that maximize the efficiency and cost-effectiveness of a microfluidic heating system. These generalized models are expected to apply to any source, materials, and geometry for which the optical and material properties are known.

© 2011 Elsevier B.V. All rights reserved.

### 1. Introduction

The ability to control the temperature of liquids in a microscale environment is often a critical functional requirement in the design of miniaturized systems for biological analyses. An example microfluidic application is the polymerase chain reaction (PCR), a technique used to amplify DNA template through the use of a heat-stable polymerase enzyme and thermal cycling [1–3]. This process is most efficiently executed at multiple, precisely maintained temperatures with minimal transition times. Further, inducing elevated temperatures is commonly utilized for cell lysis [4,5], protein denaturation [6], heat shock DNA transformation [7], and activating the lambda red genetic pathway for homologous recombination experiments [8]. Generating reliable dynamic thermal conditions is also important for applications such as melting curve analysis and enzyme reaction control [9].

Many of these temperature-dependent biological processes have undergone miniaturization, heralding both the benefits and challenges of scaling. Small volumes not only preserve precious reagents, therefore reducing costs, but also reduce the sample's thermal mass, or heat capacity, enabling faster thermal response and lower power consumption compared to macroscale equivalents. On the other hand, typical microfluidic geometries exhibit

high surface-area-to-volume ratios, resulting in heat transfer dominated by conduction. This can present unfavorable parasitic heat loss and create problems for isolating heat generation on-chip.

The task of integrating heating systems with microdevices has been carried out at various degrees of accuracy and complexity. The implementation and effectiveness of the heat transfer modes: conductive, convective, and radiative, depend on material selection, fabrication allowances, and the performance requirements of the respective application. While many microfluidic devices have increased throughput with smaller sample volumes, they continue to rely on conventional conductive heating from macroscale thermoelectric heating blocks [10]; however, on-chip resistive heaters [1], circulating hot air (Roche LightCycler), and infrared radiation-based thermocycling [2] are becoming widely used and offer alternative methods for faster, more controllable heating.

Of the heat transfer modes for microchip temperature control, radiative heating offers several unique advantages. By matching a source of radiation to strongly absorptive wavelengths of a particular liquid, radiative heating efficiently transfers energy to the medium of interest and can yield rapid temperature ramping (e.g., 32 °C/s for water [11]). Additionally, an external source keeps microchip design and fabrication simple and mediates the risks of adsorption and reaction inhibition due to incompatible materials embedded in the device, as found in other microfluidic heating schemes [1]. The external source also makes a disposable chip platform more feasible. The Landers group has pioneered the use of radiative, or non-contact, temperature cycling for genetic analysis instrumentation. Volumes of approximately 270 nL can be cycled 25 times with a tungsten filament lamp in only 5 min for high-speed

\* Corresponding author at. Georgia Institute of Technology, Department of Mechanical Engineering, 315 Ferst Drive, IBB Building, Rm 2103, Atlanta, GA 30332, USA.

E-mail address: [christopher.phaneuf@gatech.edu](mailto:christopher.phaneuf@gatech.edu) (C.R. Phaneuf).

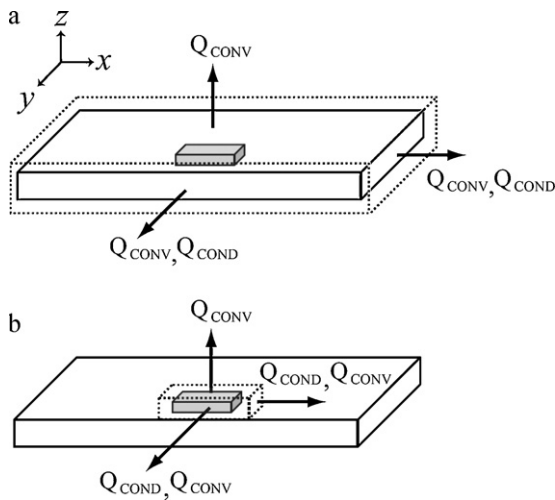


Fig. 1. Control volumes.

PCR. Other developments in radiative heating include the work of Yasuda [11] and Faris [12], using infrared laser radiation to perform real-time PCR in 10–30 nL droplets suspended in mineral oil with amplification times of 3.5 and 6 min, respectively. This technology represents great potential for fast, high-throughput implementations of temperature-dependent processes.

Designing and scaling such systems demands the ability to predict the thermal behavior for a particular microchip and radiation source in order to select the most appropriate geometries and components. Therefore, it is crucial to have accurate thermal modeling methods for all modes of heat transfer as they relate to the sample and its microenvironment. Previous work on glass PCR devices towards optimizing reaction chamber design involved heat transfer analysis that modeled the liquid volume and immediately surrounding substrate as an “effective medium” for a lumped capacitance treatment [13]. This approach is limited to cases in which the microchip substrate is heated in conjunction with the liquid and lacks a means of determining the theoretical radiation input, instead relying on tracing experimental data to back-calculate the power input.

Here we present a generalized approach to modeling the steady state and transient behavior for radiative heating in a microchip. Specifically, we use optical modeling to determine the theoretically absorbed input radiation. Then we apply closed-form analytical equations and finite element methods to model the thermal responses for specific cases of liquid water in glass and polymer microfluidic devices irradiated by broadband blackbody or monochromatic sources. We compare these models with experimental measurements. These generalized models are expected to apply to any source, materials, and geometry for which the optical and material properties are known.

## 2. Theory

We seek to model the thermal response of a prototypical microfluidic system, such as those used for the polymerase chain reaction, subjected to a radiative source. In a generalized case, this system involves a sample chamber surrounded by a material, as shown in Fig. 1. One can draw a control volume in two ways: (1) around both the chamber and immediately surrounding material (Fig. 1a), to be referred to as the effective medium approach, or (2) localized to the chamber (Fig. 1b).

Since virtually all microfluidic devices are fabricated with thin substrates, heat transfer out of the plane ( $z$ -direction) is dominated by convection. In-plane heat transfer ( $x$ - $y$  plane) will involve both

conduction and convection and the relative dominance of one or the other depends heavily on the substrate material. Without making any presumptions regarding the appropriateness of a particular model, the respective approaches for the two control volumes will be discussed in detail.

### 2.1. Effective medium approach

One possible approach to the thermal modeling of a microchamber undergoing radiative heating is based on the assumption that both the liquid sample and surrounding material are at a uniform temperature. This simplification is illustrated in Fig. 1a and has known boundary conditions. This allows a lumped capacitance treatment, for which an energy balance is applied as

$$V\rho c_p \frac{dT}{dt} = Q_{rad,in} - Q_{cond,out} - Q_{conv,out} - Q_{rad,out}, \quad (1)$$

where

$$Q_{cond,out} = \frac{k_s A_{cond} \Delta T}{L}, \quad (2)$$

$$Q_{conv,out} = h A_{conv} \Delta T, \quad (3)$$

and

$$Q_{rad,out} = F A_t \varepsilon_s \sigma (T^4 - T_\infty^4). \quad (4)$$

With the exception of  $Q_{rad,in}$ , the terms of the energy balance differential equation are detailed in previous literature that describes the optimization of a glass microchip design [13]. Briefly,  $T$  is the temperature,  $V$  is the total volume of the heated region, and material properties such as density,  $\rho$ , and specific heat at constant pressure,  $c_p$ , which apply to the entire “effective medium,” are calculated with mass-weighted averages of the constituent liquid and solid properties.  $Q_{cond,out}$  is the conduction losses to unheated parts of the microchip (if applicable), given by Eq. (2) in which  $k_s$  is the thermal conductivity of the substrate,  $A_{cond}$  is the cross-sectional area at the interface, and  $L$  is the length of the conducting region in the direction of conduction.  $Q_{conv,out}$  is the free convection out, given by Eq. (3) where  $A_{conv}$  is the total convecting surface area of the medium and  $h$  is the heat transfer coefficient. This is calculated from the Nusselt number, which is found using an empirical correlation with the Rayleigh and Prandtl numbers based on the particular geometry of the convecting body.  $Q_{rad,out}$  is the radiation out, calculated by Eq. (4), where  $F$  is the shape factor,  $A_t$  is the total exposed area of the control volume,  $\varepsilon_s$  is the emissivity of the medium, and  $\sigma$  is the Stefan–Boltzmann constant.

The theoretical radiation into the control volume,  $Q_{rad,in}$ , is calculated from the optical properties of the source and the geometric and absorptive properties of the absorbing media. For the source, spectral irradiance data is scaled by integrating over its full spectrum and equating it to the known total power output. This yields the scaled spectral power distribution,  $P_0(\lambda)$ . The losses due to reflection at the air–glass and glass–water interfaces were calculated to be 4% and 0.5% respectively based on simplified reflection coefficient equations for near-normal incidence. Using absorption coefficients,  $\alpha(\lambda)$ , of the absorbing media and the path length,  $l$ , through which the radiation travels, the absorbed power  $P_{abs}(\lambda)$  is given by the Beer–Lambert law as  $P_{abs}(\lambda) = P_0(\lambda)(1 - 10^{-\alpha(\lambda)l})$ . This is integrated with respect to wavelength and, in the case that the focal spot is larger than the control volume, adjusted for the incident area and, if necessary, the intensity distribution to provide the radiative power into the control volume. For the spatial and temporal scales we are concerned with in this study, the quasi-Gaussian distribution of the laser and the lamp focal spot were assumed uniform.  $Q_{rad,in}$  is then the sum for all absorbing bodies that constitute the effective medium.

Considerations when determining the radiant power from an incandescent lamp include the power supply dependent spectral curve, which shifts towards blue with higher power. Our calculations accounting for this shift within our practical power range indicate a negligible effect (e.g., less than 5%) on the final absorbed radiation calculation.

Eq. (1) can first be solved algebraically for the steady state temperature of the effective medium ( $(dT/dt)=0$ ). The energy balance can be solved for  $T(t)$  using an explicit numerical method such as Runge–Kutta to calculate the transient response.

## 2.2. Finite element approach

If one instead assumes that thermal gradients in the substrate cannot be neglected, the control volume must be drawn as in Fig. 1b. This is appropriate for cases when the substrate is not absorbant for the spectral range of the source or the spatial distribution of the radiation is highly localized to the chamber. Modeling such a scenario is best accomplished with finite element analysis.

The geometry of the microdevice is created in finite element software, or imported from solid modeling software, and broken up into subdomains and boundaries, each of which is given the specific parameters of the problem. Subdomains are assigned appropriate material properties, along with a heat generation term is calculated from the same optical modeling used for determining  $Q_{rad,in}$  in the previous approach, which must then be divided by the volume of the absorbing region for units of  $W/m^3$ . For the exterior boundary conditions, a heat transfer coefficient,  $h$ , is calculated from the Nusselt number, as earlier described. For the interior boundaries, continuity is applied.

The transient response is then solved from a set of differential equations for the subdomains, the external boundaries, and internal boundaries. The subdomains are governed by

$$\delta_{ts} \rho c_p \frac{\partial T}{\partial t} + \nabla \cdot (-k \nabla T) = Q, \quad (5)$$

where  $\delta_{ts}$  is the time scaling coefficient which is equal to 1 for the transient case,  $\rho$  is the material density,  $c_p$  is the heat capacity at constant pressure,  $T$  is temperature,  $t$  is time,  $k$  is the thermal conductivity of the material, and  $Q$  is the heat generation. External boundaries are defined as

$$-\mathbf{n} \cdot (-k \nabla T) = h(T_{inf} - T) + \varepsilon \sigma (T_{amb}^4 - T^4), \quad (6)$$

where  $\mathbf{n}$  is a normal vector,  $k$  is the thermal conductivity,  $T$  is the temperature,  $h$  is the heat transfer coefficient,  $T_{inf}$  and  $T_{amb}$  are the external ambient temperatures,  $\varepsilon$  is the surface emissivity, and  $\sigma$  is the Stefan–Boltzmann constant. For the internal boundaries

$$-\mathbf{n}_u \cdot (-k_u \nabla T_u) - \mathbf{n}_d \cdot (-k_d \nabla T_d) = 0, \quad (7)$$

where  $\mathbf{n}$  is a normal vector,  $k$  is the thermal conductivity, and  $T$  is temperature. The  $u$  and  $d$  subscripts refer to the two different subdomains that meet at the internal boundary.

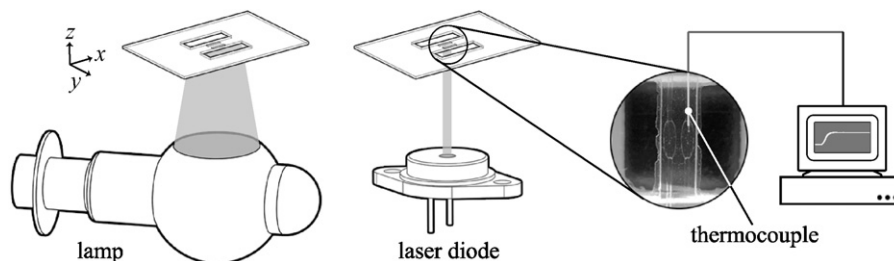


Fig. 3. Experimental setup (not to scale). Blackbody tungsten-filament lamp (left) and monochromatic infrared laser diode (center) with a photograph of the inserted thermocouple (right). Laser collimation optics not shown.

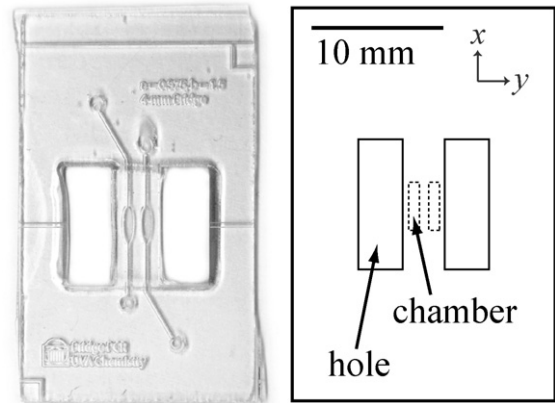


Fig. 2. Glass microchip (left) and analogous modeled geometry (right).

Once initial conditions are set, the geometry is meshed and the problem can be evaluated for a specified duration. A mesh sensitivity test should be performed by refining the mesh until the results do not change between successive simulations.

## 3. Experimental design

The above described models were implemented and experimentally validated for radiative heating in glass and plastic microchips coupled to blackbody and monochromatic radiation sources. The glass device is a two-chamber microchip designed for PCR with 500 nL samples, courtesy of James Landers at the University of Virginia and shown in Fig. 2. The device is made of borosilicate glass and was fabricated using standard photolithography, wet-etching, and thermal bonding techniques. The plastic device is made of poly (methyl methacrylate) (PMMA) and possesses geometry similar to the glass device. It was fabricated in-house by laser etching the features with a CO<sub>2</sub> laser cutter (VersaLASER, VLS3.50). The dimensions were confirmed with surface profilometry (Dektak 3030) and the enclosed two-layer device was thermally bonded in boiling water [14].

We used a 50 W tungsten-filament incandescent projector lamp (Eiko, CXL/CXR 8 V 50 W) for our blackbody source and a 600 mW 1450 nm laser diode (Hi-Tech Optoelectronics, LMD-1450-600-33) for our monochromatic source, which was selected to match an absorption band of water. This experimental setup is depicted in Fig. 3. For the lamp, the total power output is calculated from the electrical power supplied,  $P = V \times I$ , where  $V$  is the voltage and  $I$  is the current. Spectral data for determining the absorbed radiation was transcribed from a spectral irradiance curve with a resolution of 25 nm for the range from 300 to 5000 nm. For the laser, the power output is a known function of the supply current and was confirmed with a power meter. The Gaussian beam profile of the laser diode was sampled with a spectral resolution of 0.5 nm for the short-wavelength infrared range of 1440–1460 nm.

Since the blackbody radiation of our lamp melts PMMA and therefore excludes this combination from practical testing, three cases were modeled and tested experimentally: (1) lamp heating of water in glass, (2) laser heating of water in glass, and (3) laser heating of water in polymer. Temperatures were kept between the ambient 25 °C and 100 °C to avoid damaging the PMMA microchip, which has a glass transition temperature of approximately 105 °C. Therefore, the radiative sources were not always operated at full power.

The effective medium and finite element approaches were implemented for each case. As earlier mentioned, the thin substrates of most microfluidic devices results in negligible thermal gradients across the thickness ( $z$ ), leaving convection as the primary mode of heat loss. On the other hand, thermal gradients across the width ( $y$ ) and length ( $x$ ) of a device may not be sufficiently uniform for the application of the effective medium assumption. As a preliminary assessment of this temperature uniformity, a three-dimensional finite difference model, programmed in computation software Engineering Equation Solver (EES) using Eq. (1), calculated the steady state temperatures for a set of nodes representing the heating cases for heating in a glass chip for the lamp and laser.

The transient solutions for each case were first calculated by applying the effective medium assumption and were solved using a fourth and fifth order Runge–Kutta method. The cases were then solved using finite element software COMSOL Multiphysics. Simplified geometry of the glass and polymer microchips was created as shown in Fig. 2 (right). The reaction chambers were specified as water volumes and were assigned heat generation values based on the theoretical absorbed radiation. For the case of the lamp heating in a glass microchip, the glass and water were both assigned heat generation values. For the laser heating in glass and polymer chips, only heat generation in the liquid reaction chambers needed to be specified since the absorption of the 1450 nm laser output by the solid substrates is negligible. The finite element solver was run for a time domain of 60 s and temperature values were recorded every 0.01 s at 10 equally spaced points along the centerline of the reaction chamber. The values at the 10 points were then averaged to obtain the mean temperature for the liquid chamber. A mesh sensitivity test revealed no need for refinement of the auto-generated mesh.

For experimental validation, lamp heating was performed at an intermediate power level of 9.3 W as specified in the models. Laser heating in glass was performed at the full power of 620 mW. For heating in the polymer device, the power was reduced to 300 mW to prevent the heated water from causing channel deformation due to thermal expansion and material softening above the glass transition temperature.

The lamp was powered with a variable power source and focusing was achieved with an ellipsoidal retroreflector, which provided a roughly circular focal spot with a diameter of about 10 mm. The laser was driven with a low-noise current source (Thorlabs, ITC133) and controlled with a 10 Hz PWM signal output from a National Instruments LabView program. The diverging beam is collimated with an aspheric molded glass lens (Thorlabs, A230TM-C), producing a 5 mm by 2 mm elliptical spot. The inherent ramping of output intensity of each source was measured using an optical power meter (Thorlabs, PM10-3) and rise times were considered negligible compared to the transient heating time scales.

Temperature was measured using a calibrated T-type micro-thermocouple (Physitemp Instruments, T-240C), a thermocouple-to-analog converter (Omega, TAC80B-T), and an analog amplifier. Measurements were recorded with LabView and data collection was synchronized with the power supplies for the lamp and laser using a digital output from our data acquisition hardware. The thermocouple, which has a 0.003" diameter and response time of

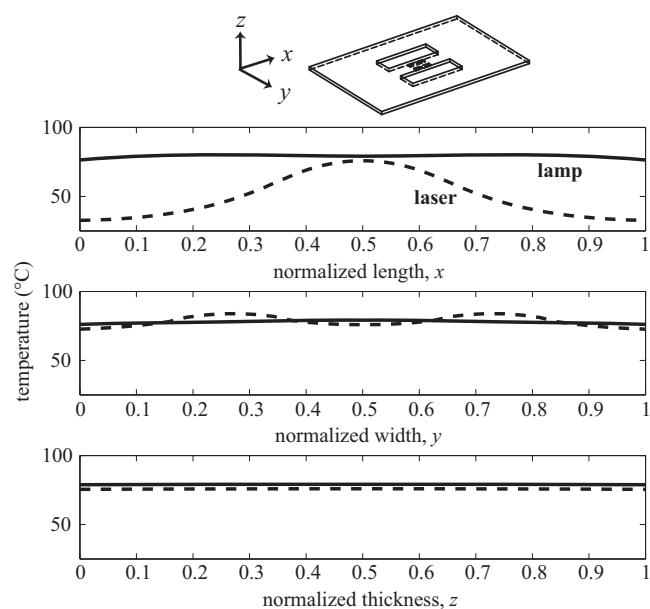


Fig. 4. Modeled steady state temperature profiles over normalized dimensions of the water-filled glass microchip for lamp (solid) and laser (dashed) heating. Larger thermal gradients are observed over the length and width for the laser simulation compared to the more uniform profiles for the blackbody lamp heating.

3–4 ms, was inserted into the reaction chamber through an inlet channel, as pictured in Fig. 3. The thermocouple tip was positioned with minimal protrusion into the chamber to avoid direct irradiation. With an insertion length of 0.5 mm and a diameter of 0.06 mm, the thermocouple occupied only 0.5% of the total chamber volume and had a negligible influence on the thermal mass.

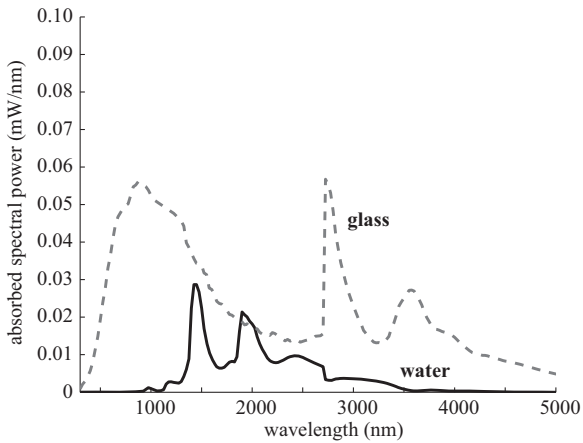
#### 4. Results and discussion

The preliminary tests of the appropriateness of the effective medium approach using finite difference analysis to calculate steady state temperatures is shown in Fig. 4, which reveals the temperature profiles for lamp and laser heating in glass over the length, width, and thickness of the whole device. While heating with the blackbody source results in roughly uniform temperatures, the laser heating profiles show more localized heating behavior inconsistent with the prerequisite condition for the effective medium assumption.

The reasons for this behavior are elucidated in Table 1, which summarizes the absorbed radiation values for the lamp and laser heating in the glass microchip. Despite the much greater efficiency of laser heating an aqueous sample, the lamp's higher power output and significant absorption by the glass results in a device of uniform temperature and conductive losses from the chamber are therefore minimized. Conversely, the laser heating is localized in the liquid medium because of the smaller focal spot and the transparency of the microchip substrate to the infrared radiation. This results in greater heat sinking by the substrate, i.e., in-plane conductive heat loss.

Table 1  
Percentage of total radiation absorbed.

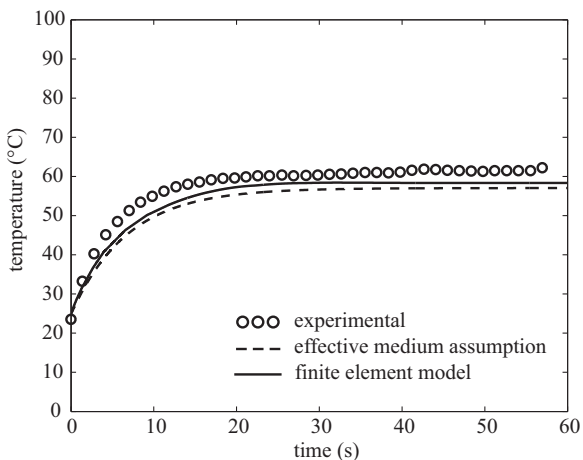
Source	Absorbing medium	
	Water	Glass
Lamp	2%	10%
Laser	70%	1%



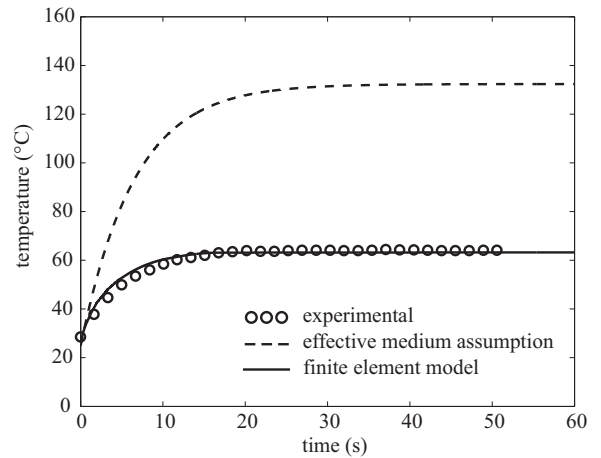
**Fig. 5.** Blackbody lamp radiation absorbed by water (solid) and glass (dashed). 5× more radiation is absorbed by the glass substrate than the water when irradiated by a blackbody source over an area larger than the chamber.

Fig. 5 shows a further examination of the absorbed spectral power from the lamp as absorbed by both water and glass. Although the glass is not quite as efficient in absorbing the blackbody radiation per unit area, it experiences a larger area of exposure to the lamp output and in turn absorbs much more power than the water. Since the equivalent data for the laser would appear as a near vertical line at 1450 nm for absorption by water and a negligible peak for glass absorption, it was excluded from the plot.

The optical characteristics for the various heating cases and the results of the uniformity testing suggested the use of finite element methods to capture the localized heating by our laser. The transient models are compared to experimental data in Figs. 6–8. As a metric for the accuracy of the models when compared to the experimental data, root mean square deviation was calculated as  $\sqrt{(1/n) \sum |T_{exp} - T_{model}|^2}$ . For lamp heating of glass, shown in Fig. 6, the effective medium model exhibits a deviation of 4.54 °C while the finite element model matches slightly better with a deviation of 3.10 °C. For laser heating in glass, the effective medium model deviates considerably with a mean difference of 61.17 °C, which is to be expected from the temperature uniformity results of Fig. 4. The finite element model offers a much better correlation with a deviation of 1.37 °C. Similarly, for laser heating in our polymer device, the effective medium model is 59.25 °C off while the finite element model deviates by an average of 3.14 °C.



**Fig. 6.** Lamp heating in a glass microchip. Root mean square deviation from experimental data: effective medium = 4.54 °C, finite element = 3.10 °C.



**Fig. 7.** Laser heating in a glass microchip. Root mean square deviation from experimental data: effective medium = 61.17 °C, finite element = 1.37 °C.

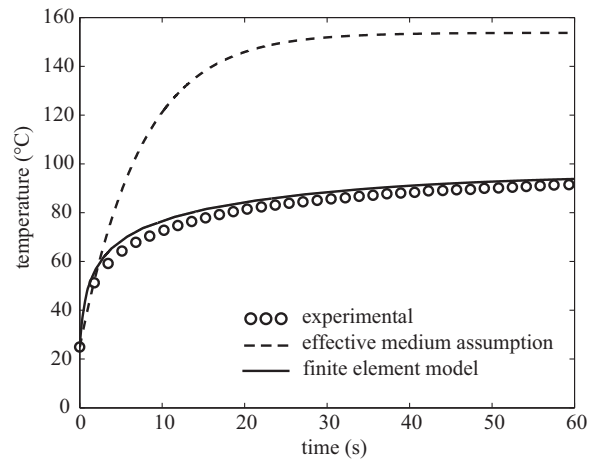


**Fig. 8.** Laser heating in a polymer microchip. Root mean square deviation from experimental data: effective medium = 59.25 °C, finite element = 3.14 °C.

With the lamp powered at 9.3 W, which corresponds to the data in Fig. 6, the radiation absorbed by the water is approximately 20 mW while the glass absorbs 110 mW and results in a steady state temperature of 62 °C. To compare, the laser operating at its full power of 620 mW imparts 435 mW to the water but the sample only reaches a steady state temperature of 64 °C as shown in Fig. 7. Without a heated substrate, the liquid volume suffers from significant conductive losses and the ratio of steady state temperature to power absorbed by the water is much lower than that for lamp

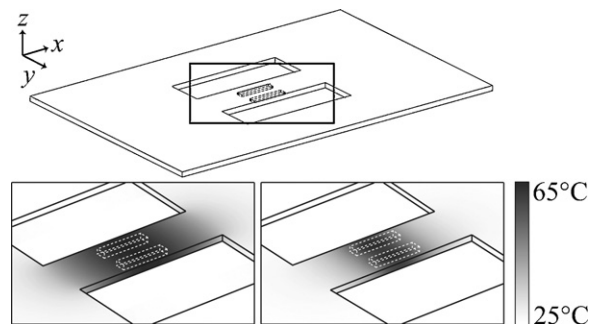


**Fig. 9.** Thermal gradients for lamp (left) and laser (right) heating in glass. The temperature uniformity of the substrate surrounding the chambers for heating with the lamp is contrasted with the localized hotspots for heating with the laser.

heating. The less thermally conductive polymer microchip exhibits reduced conductive heat loss and with the laser power at less than half of that used for glass chip heating, the steady state temperature is a much higher 95 °C as shown in Fig. 8. Post-processing of the finite element data can be seen in Fig. 9, providing a visualization of the thermal gradients of the cases of lamp and laser heating in the glass microchip model.

Small discrepancies between the modeled thermal responses and the experimental data can be attributed to the difficulty in achieving the perfect alignment and spacing inherent in the modeled cases. Additionally, the adjustments made for the theoretical intensity distribution of the sources will be approximations of the actual distributions.

## 5. Conclusion

The optical and heat transfer components of our analysis are valuable guides in the implementation of radiative heating in a microchip. While the lumped capacitance treatment can be a simple and accurate method for a narrowly defined case, finite element methods allow a more generalized treatment of any control volume. Using the predicted values for absorbed radiation from the optical model, the finite element approach yielded root mean square deviations from experimental data of 3.10 °C, 1.37 °C, and 3.14 °C for lamp heating in a glass device and laser heating in a glass and polymer device, respectively.

By delineating the radiative contributions of a particular light source to the heating of liquid and solid volumes, the optical modeling provides not only inputs for the heat transfer analysis but also key insights into the efficacy of radiative heating for the variety of microfluidic design permutations. In many ways, heating with a blackbody radiator is viable for a thermally stable substrate because it mimics conventional contact-based heating by directly heating both the liquid and substrate while retaining the advantages of the non-contact method. But the limitations of blackbody heating for applications demanding lower substrate cost, higher throughput, and greater spatial control make the use of a laser a more capable option.

With the ideal type of source selected, finite element modeling is crucial for anticipating the required power input and for refining

the choice of materials and geometric parameters. The demonstrated accuracy of these methods should prove to be sufficient for a single iteration design of any microfluidic radiative heating system.

## References

- [1] C.N. Liu, N.M. Toriello, R.A. Mathies, Multichannel PCR-CE microdevice for genetic analysis, *Analytical Chemistry* 78 (15) (2006) 5474–5479.
- [2] A.F.R. Huhmer, J.P. Landers, Noncontact infrared-mediated thermocycling for effective polymerase chain reaction amplification of dna in nanoliter volumes, *Analytical Chemistry* 72 (21) (2000) 5507–5512.
- [3] C.-S.J. Hou, M. Godin, K. Payer, R. Chakrabarti, S.R. Manalis, Integrated micro-electronic device for label-free nucleic acid amplification and detection, *Lab on a Chip* 7 (3) (2007) 347–354, doi:10.1039/b617082j.
- [4] R.H. Liu, J. Yang, R. Lenigk, J. Bonanno, P. Grodzinski, Self-contained, fully integrated biochip for sample preparation, polymerase chain reaction amplification, and DNA microarray detection, *Analytical Chemistry* 76 (7) (2004) 1824–1831, doi:10.1021/ac0353029.
- [5] S.-W. Yeung, T.M.-H. Lee, H. Cai, I.-M. Hsing, A dna biochip for on-the-spot multiplexed pathogen identification, *Nuclear Acids Research* 34 (18) (2006) e118-.
- [6] A.W. Chow, Protein separations, in: *Microchip Capillary Electrophoresis*, 2006, pp. 145–158, doi:10.1385/1-59745-076-6:145.
- [7] S. Li, L.M. Anderson, J.-M. Yang, L. Lin, H. Yang, DNA transformation via local heat shock, *Applied Physics Letters* 91 (1) (2007) 013902–13903.
- [8] K. Murphy, K. Campellone, Lambda red-mediated recombinogenic engineering of enterohemorrhagic and enteropathogenic *E. coli*, *BMC Molecular Biology* 4 (1) (2003) 11.
- [9] Y. Tanaka, M.N. Slyadnev, A. Hibara, M. Tokeshi, T. Kitamori, Non-contact photothermal control of enzyme reactions on a microchip by using a compact diode laser, *Journal of Chromatography A* 894 (1–2) (2000) 45–51, doi:10.1016/S0021-9673(00)00593-8.
- [10] M. Slyadnev, M. Lavrova, M. Erkin, V. Kazakov, A. Ganeev, Development of a multireactor microfluidic system for the determination of dna using real-time polymerase chain reaction, *Journal of Analytical Chemistry* 63 (2) (2008) 192–198, doi:10.1007/s10809-008-2015-2.
- [11] H. Terazono, A. Hattori, H. Takei, K. Takeda, K. Yasuda, Development of 1480 nm photothermal high-speed real-time polymerase chain reaction system for rapid nucleotide recognition, *Japanese Journal of Applied Physics* 47 (6) (2008) 5212.
- [12] H. Kim, S. Vishniakou, G.W. Faris, Petri dish PCR: laser-heated reactions in nanoliter droplet arrays, *Lab on a Chip* 9 (9) (2009) 1230–1235, doi:10.1039/b817288a.
- [13] C.J. Easley, J.A.C. Humphrey, J.P. Landers, Thermal isolation of microchip reaction chambers for rapid non-contact dna amplification, *Journal of Micromechanics and Microengineering* 17 (9) (2007) 1758–1766.
- [14] R.T. Kelly, A.T. Woolley, Thermal bonding of polymeric capillary electrophoresis microdevices in water, *Analytical Chemistry* 75 (8) (2003) 1941–1945, doi:10.1021/ac0262964.